Electronic Supplementary Material (ESI) for New Journal of Chemistry.
This journal is © The Royal Society of Chemistry and the Centre National de la Recherche Scientifique 2023

Supplementary Information

Binary Co_9S_8-$NiCo_2S_4$ anchored on N-Doped rGO Backbone as an Efficient Bifunctional and Durable Hetero-catalyst For Overall Water-splitting in Alkaline Medium

Mubashir Ali,[a] Malik Wahid*†[a] and Kowsar Majid,*†[a]

[a] Department of Chemistry, Interdisciplinary Division for Renewable Energy and Advanced Materials (iDREAM), National Institute of Technology (NIT) Srinagar. Srinagar-190006, India.
†Authors contribute equally to this work.
Email:kowsar@nitsri.net; malikwahid15@gmail.com;

1. IR-correction, Tafel slope, and overpotential calculations:

The LSV measurements were rectified for electrolyte resistance using equation S2.

$$E_{corrected} = E - IR \quad \ldots\ldots\ldots\ldots\ldots\ldots\text{Eqn. (S2)}$$

Here, I is the measured current (A), R is the uncompensated solution resistance (ohm), and E is the potential applied (V).

The overpotentials (ɳ) are calculated using:

$$\eta = E_{corrected} - E_{rev.}$$

Where $E_{rev.}$ is the thermodynamic potential (V). On the RHE scale, $E_{rev.}$ is 0 V for HER. Therefore, the $E_{corrected}$ is equal to applied ɳ. For OER, the $E_{rev.}$ is 1.23 V vs. RHE, and the ɳ will be

$$\eta = E_{corrected} - 1.23\ V$$

Tafel plots for HER and OER are obtained from their respective LSV curves, and the Tafel slopes were calculated as per the Tafel equation:

$$\eta = a + b \log j$$

Where a, b, and j represent the Tafel constant, Tafel slope, and current density, respectively.

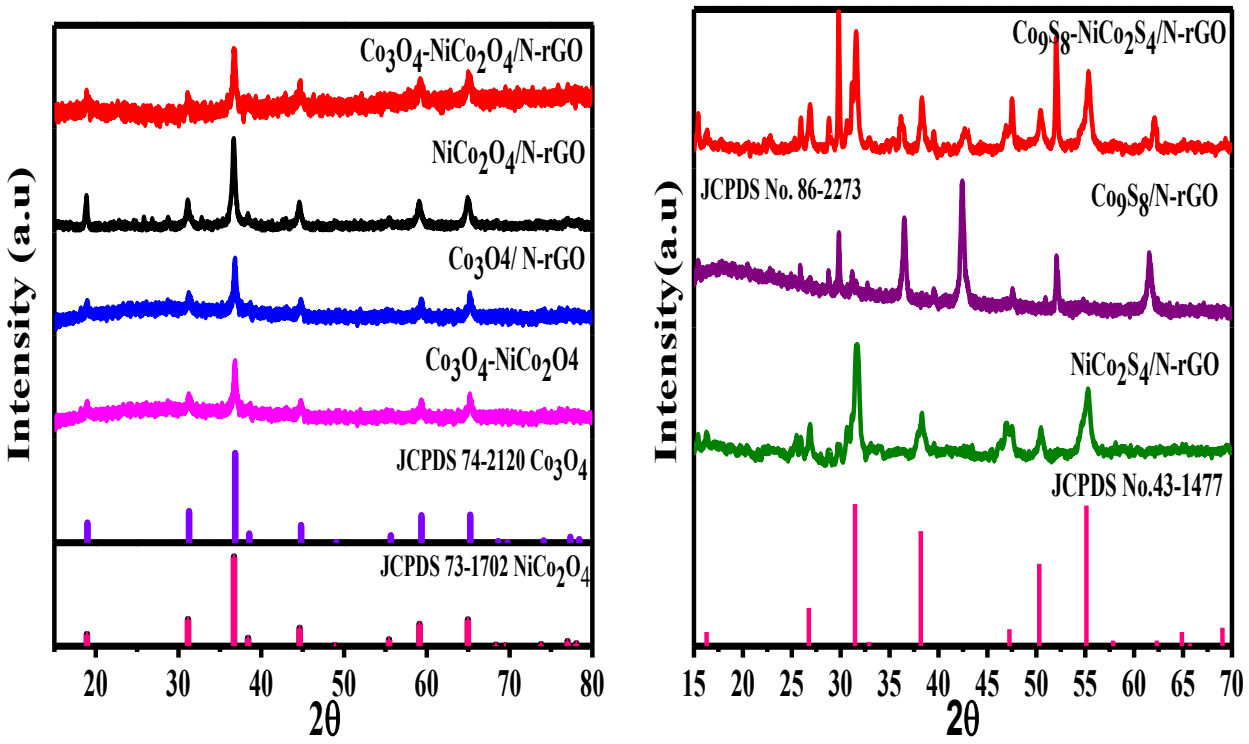

Figure S1.(a) PXRD of oxide precursor Co_3O_4-$NiCo_2O_4$/N-rGO hetero-catalyst vis-à-vis individual oxide precursors $NiCo_2O_4$/N-rGO and Co_3O_4/N-rGO and, Co_3O_4-$NiCo_2O4$ matched to respective JCPDS cards; (b) PXRD of Co_9S_8-$NiCo_2S_4$/N-rGO hetero-catalyst,and control sulphides (Co_9S_8/N-rGO, and $NiCo_2S_4$/N-rGO) matched to respective JCPDS cards.

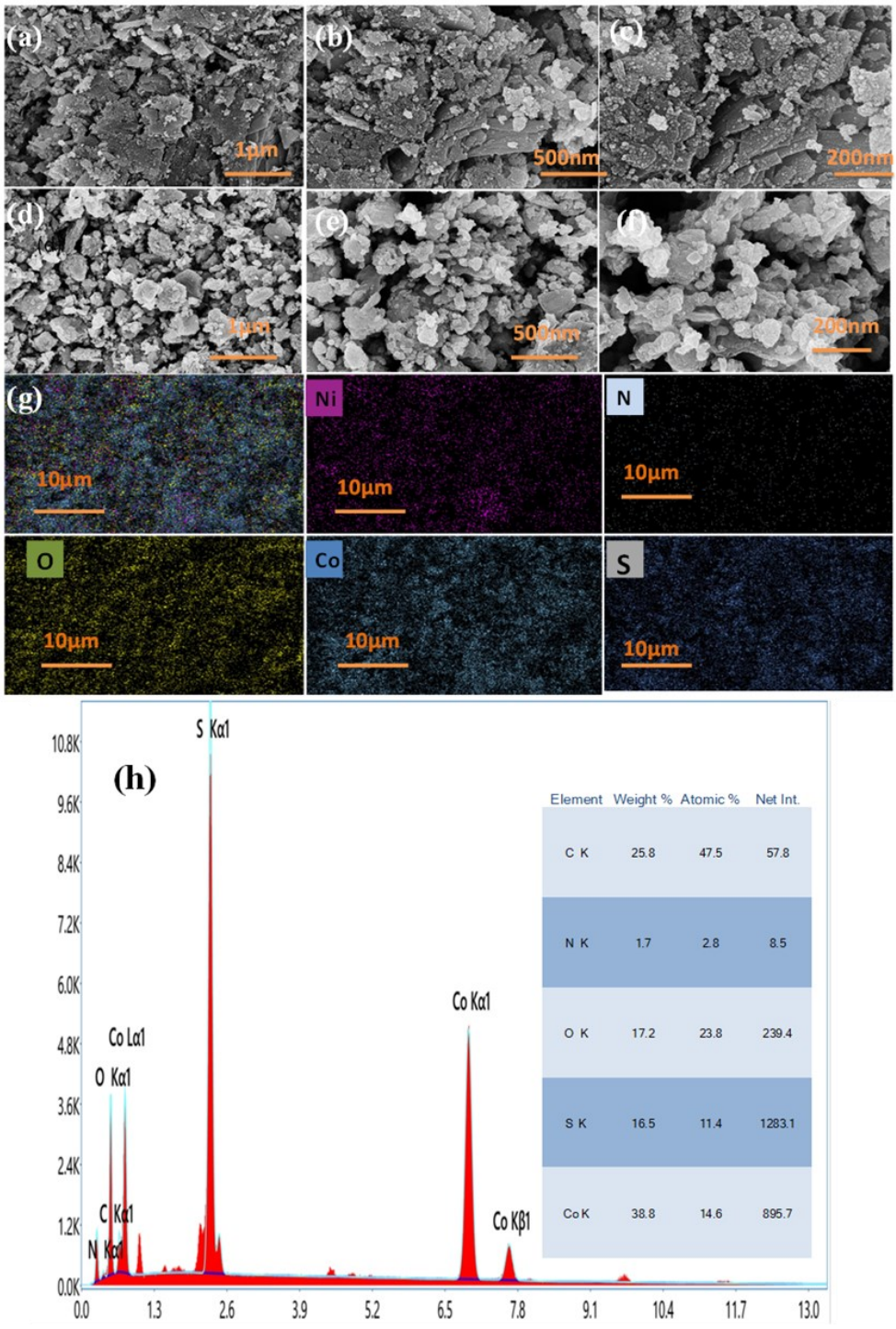

Figure S2. Comparison of morphology of control sulphide Co_9S_8/N-rGO vis-a-viscorresponding precursor oxide Co_3O_4/ N-rGO. (a), (b), (c) FESEM micrographs of Co_3O_4/ N-rGO at different magnifications; (d), (e), (f) FESEM micrographs of Co_9S_8 /N-rGO; (g) SEM elemental mapping of Co_9S_8/N-rGO;(h) EDS spectrum of Co_9S_8/N-rGO.

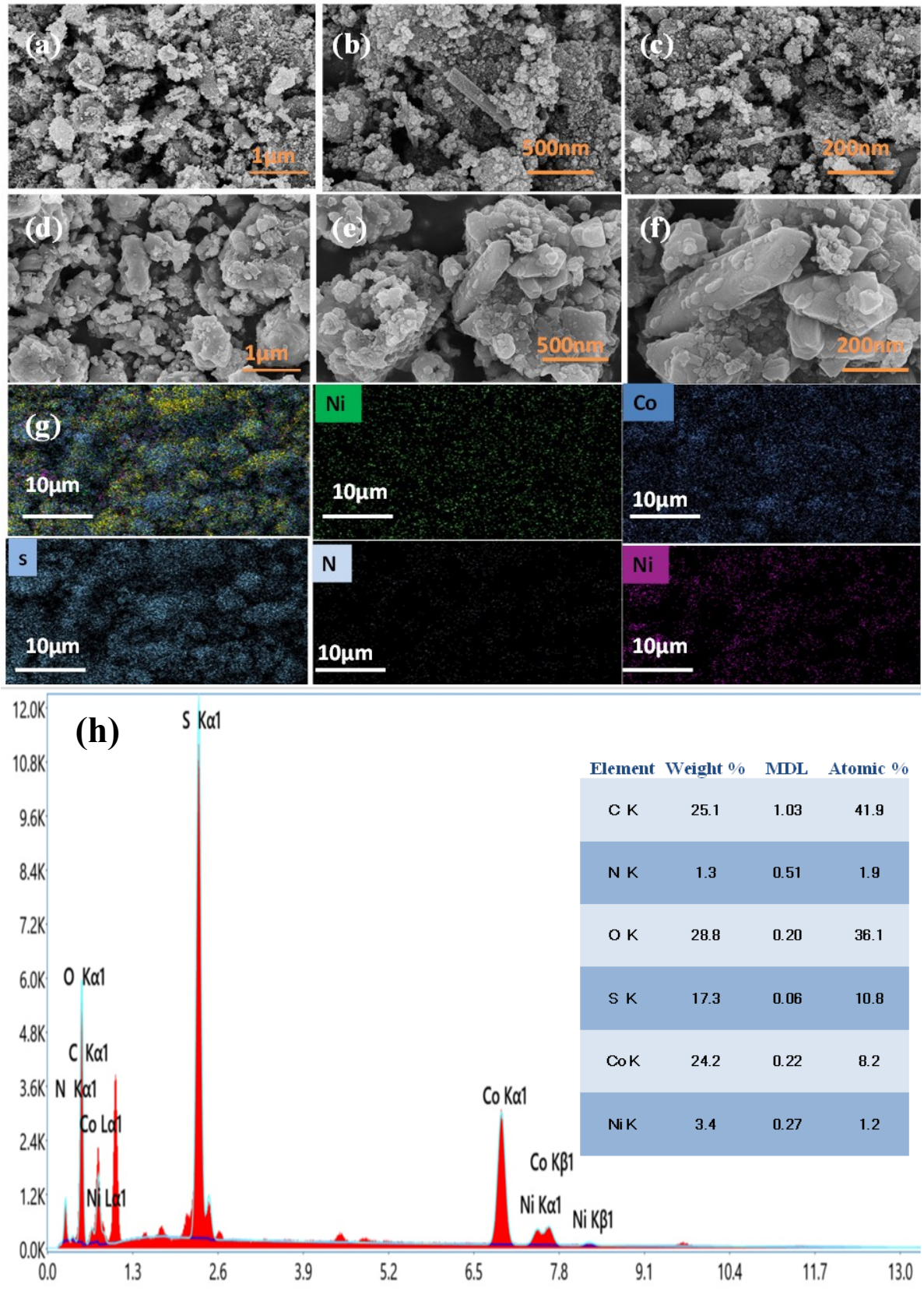

Element	Weight %	MDL	Atomic %
C K	25.1	1.03	41.9
N K	1.3	0.51	1.9
O K	28.8	0.20	36.1
S K	17.3	0.06	10.8
Co K	24.2	0.22	8.2
Ni K	3.4	0.27	1.2

Figure S3. Comparison of morphology of control sulphide$NiCo_2S_4$/N-rGO vis-a-viscorresponding precursor oxide $NiCo_2O_4$/N-rGO. (a), (b), (c) FESEM micrographs of $NiCo_2O_4$/N-rGO at different magnifications; (d), (e),(f) FESEM micrographs of $NiCo_2S_4$/N-rGO; (g) SEM elemental mapping $NiCo_2S_4$/N-rGO; (h) EDSspectrum of $NiCo_2S_4$/N-rGO.

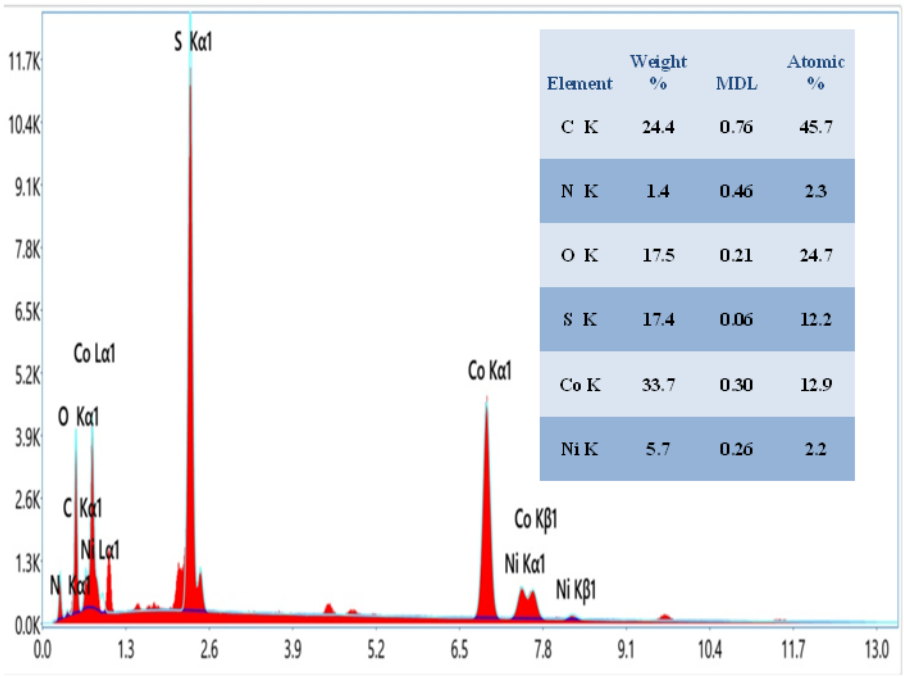

Element	Weight %	MDL	Atomic %
C K	24.4	0.76	45.7
N K	1.4	0.46	2.3
O K	17.5	0.21	24.7
S K	17.4	0.06	12.2
Co K	33.7	0.30	12.9
Ni K	5.7	0.26	2.2

Figure S4. EDS spectrum of Co_9S_8-$NiCo_2S_4$/N-rGO

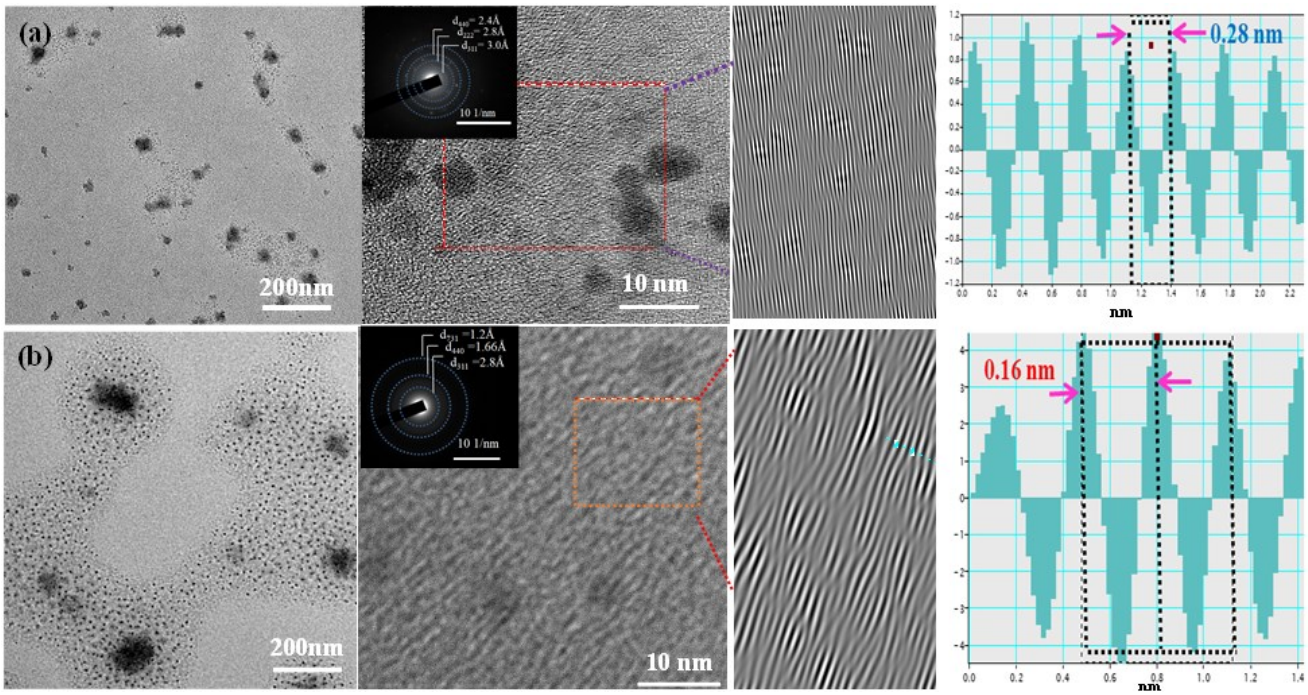

Figure S5. HRTEM analysis of Co_9S_8/N-rGO and $NiCo_2S_4$/N-rGO samples. (a) High-resolution HRTEM micrograph of Co_9S_8/N-rGO (top left), the HRTEM fringe analysis at higher magnifications with SAED pattern as inset (top middle), IFFT pattern (top right); (b) High-resolution HRTEM micrograph of $NiCo_2S_4$/N-rGO (bottom left), the HRTEM fringe analysis at higher magnifications with SAED pattern as inset (bottom middle), IFFT pattern (bottom right).

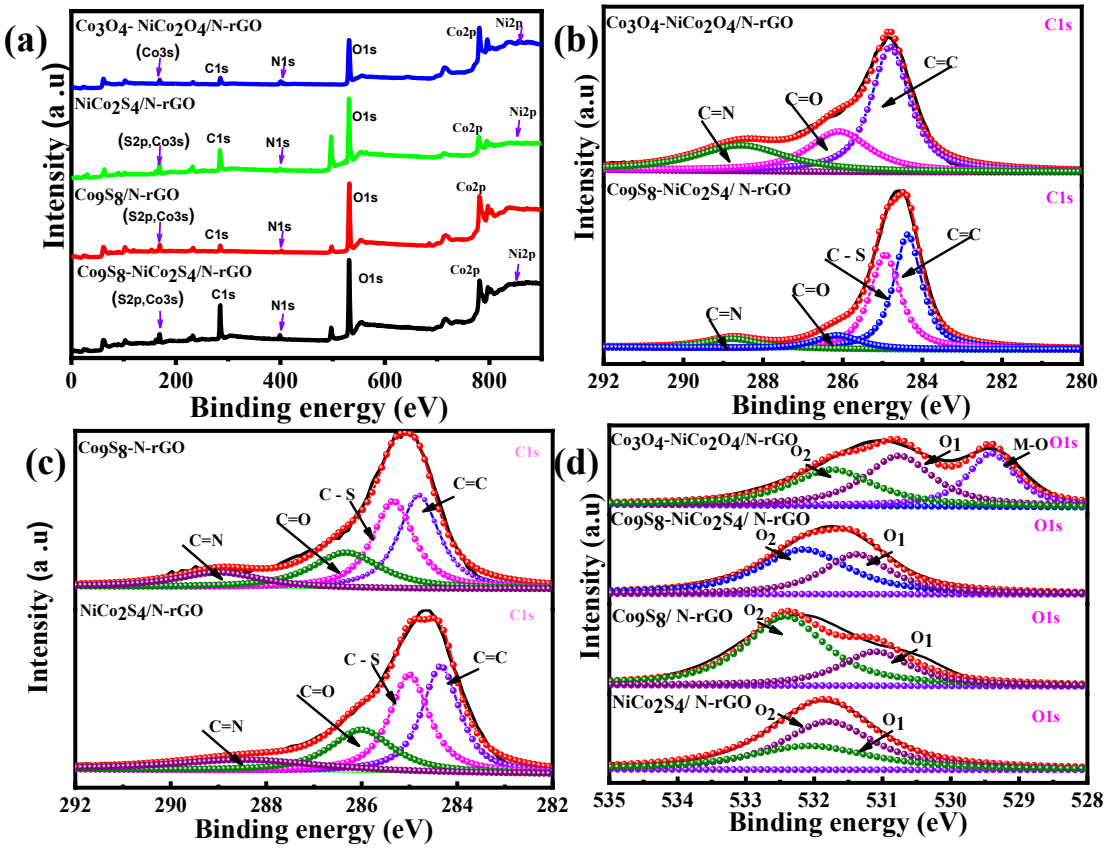

Figure S6. (a) XPS survey spectrum of Co_9S_8/N-rGO, $NiCo_2S_4$/N-rGO, Co_9S_8-$NiCo_2S_4$/N-rGO and Co_3O_4-$NiCo_2O_4$/ N-rGO depicting the presence of expected elements;Deconvoluted individual spectra: (b) C 1s comparison of Co_9S_8-$NiCo_2S_4$/N-rGO and Co_3O_4-$NiCo_2O_4$/ N-rGO ; (c) C 1s comparison of $NiCo_2S_4$/N-rGO and Co_9S_8/N-rGO, (d) O1s comparison of Co_9S_8/N-rGO, $NiCo_2S_4$/N-rGO, Co_9S_8-$NiCo_2S_4$/N-rGO and Co_3O_4-$NiCo_2O_4$/ N-rGO.

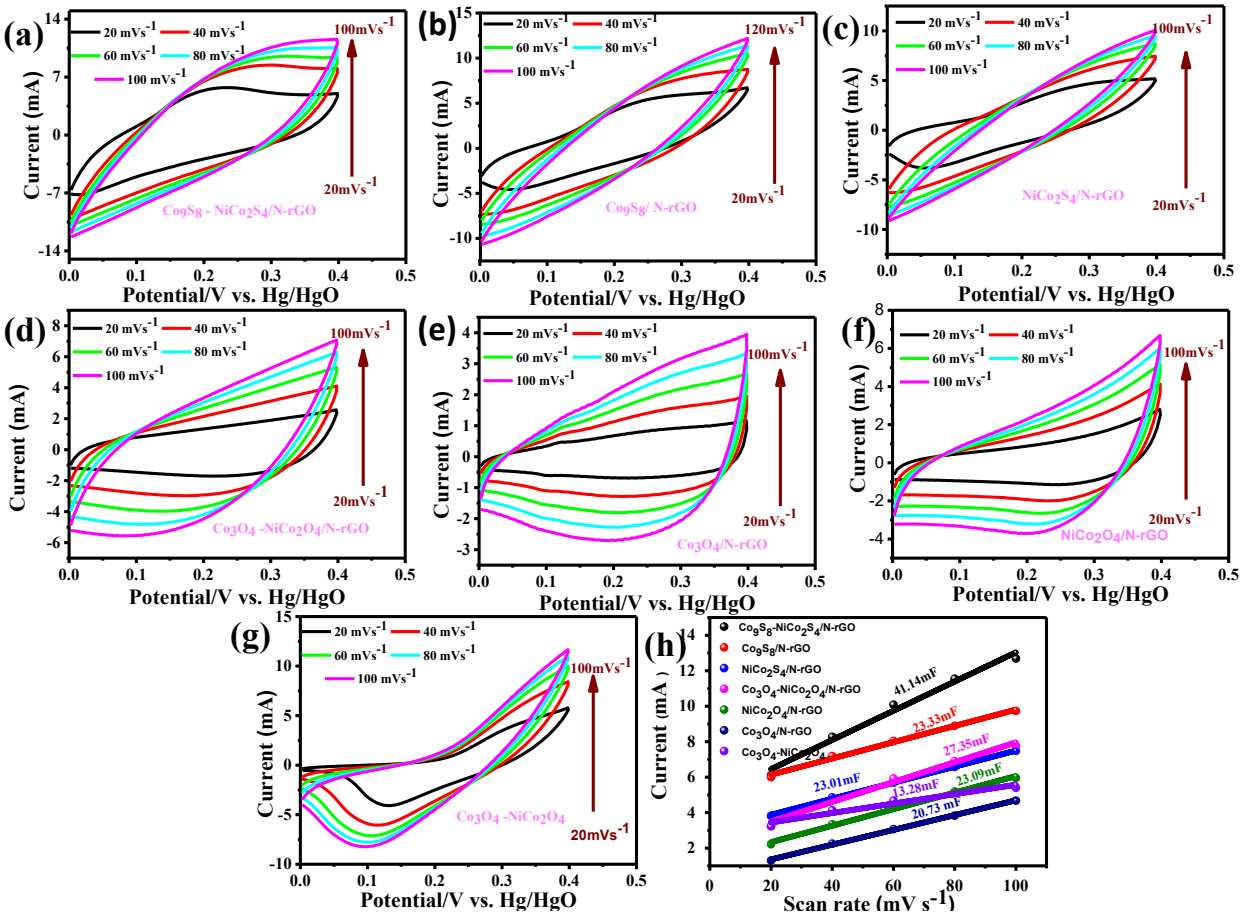

Figure S7.ECSA determination of electrocatalyst samples in 1 M KOH. Cyclic Voltammograms at different scan rates (20-100 mV sec^{-1}) in non-faradaic region: (a) Co_9S_8-$NiCo_2S_4$/N-rGO; (b) Co_9S_8/N-rGO; (c) $NiCo_2S_4$/N-rGO;(d)Co_3O_4-$NiCo_2O_4$/ N-rGO;(e) Co_3O4/N-rGO; (f) $NiCo_2O_4$/ N-rGO; (g) Co_3O_4-$NiCo_2O_4$; (h)The corresponding scan rate vs. current plot.

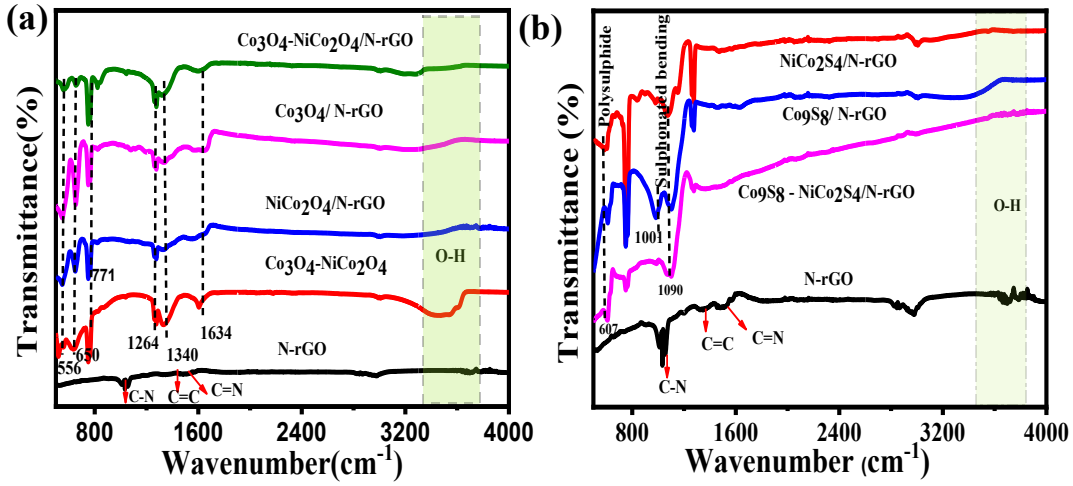

Figure S8. (a)FTIR spectra of Co_3O_4-$NiCo_2O_4$/ N-rGO sample, control oxide samples vis-à-vis N-rGO; (**b**)FTIR spectra of Co_9S_8-$NiCo_2S_4$/N-rGO sample, controlsulphidesamples vis-à-vis N-rGO.

FT-IR Details

Figure S8a: The sharp peaks at 650 cm^{-1}, 556cm^{-1} in the spectrum of Co_3O_4 are associated with the OB_3 (B represents Co^{3+} in an octahedral hole) and the ABO (A represents the Co^{2+} in a tetrahedral hole) vibrations in the spinel lattice and metal–oxygen bond vibrations in $NiCo_2O_4$[1–3]. And O-H stretching is depicted by peak is at 1634 cm^{-1}while broad absorption bands (3350- 3600 cm^{-1})corresponds to the characteristic and bending vibrations of the hydroxyl of the adsorbed H_2O[3]. The band around 771 cm^{-1} is associated with the characteristic peaks of CO_3^{2-} anions[4].

Figure S8b: The peak at 607cm^{-1} corresponds to the polysulphide group of synthesised samples. The peak at 1090 cm^{-1} can be ascribed to the S-O bonding of the sulfonated groups. The absorption peak at 628cm^{-1},751cm^{-1}(symmetric stretch) and 1120cm^{-1}(asymmetrical stretch) are assigned to the Ni-S or Co-S[5–8]. However in case of N-rGO the peaks appearing 1037cm^{-1}, 1200cm^{-1},1504cm^{-1} and 3690cm^{-1} that are attributed to the C-N,C=C, C=N respectively[3]. The broad band in the range of (3350- 3650 cm^{-1}) correspond to OH bending.

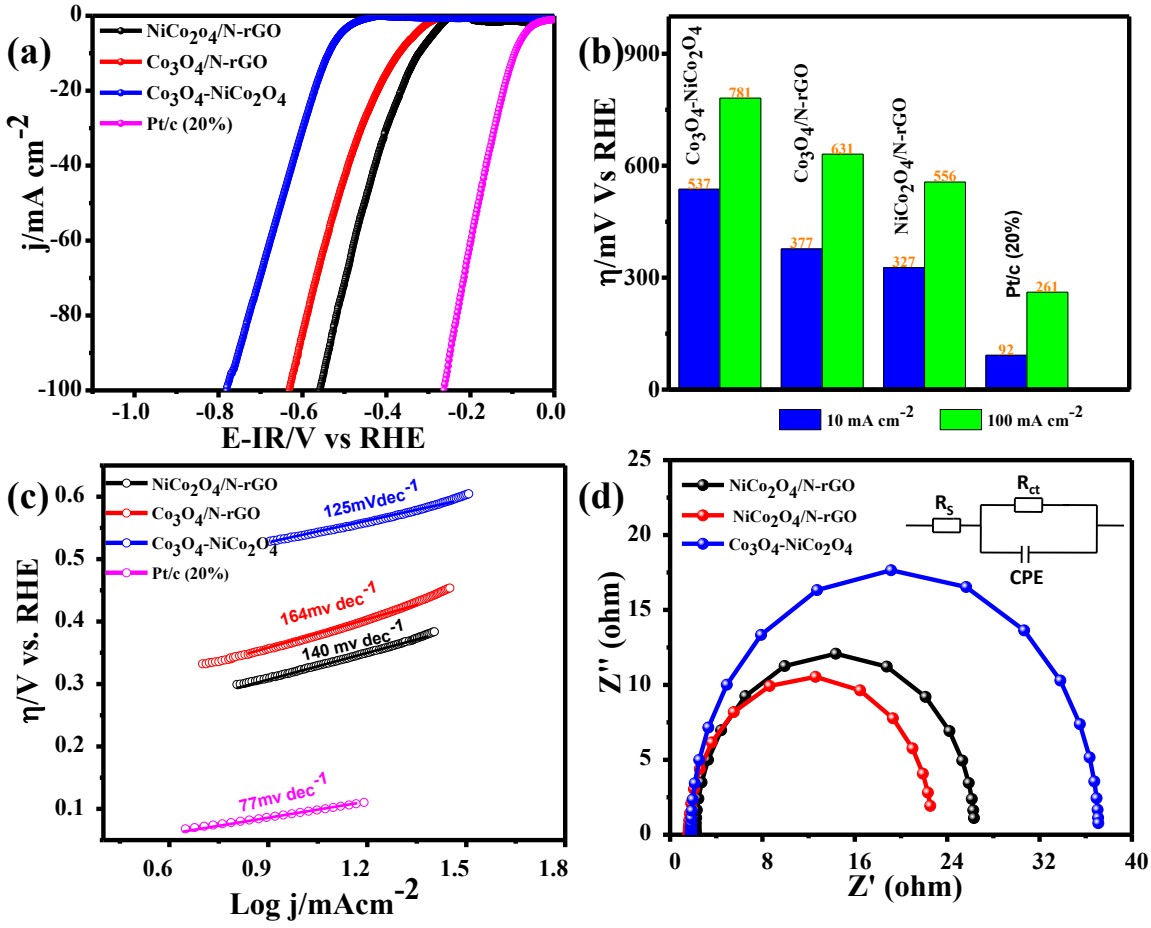

Figure S9. ElectrochemicalHER characterization of Co_3O_4-$NiCo_2O_4$, Co_3O4-rGO, and $NiCo_2O_4$/N-rGOcatalysts in 1M KOH solution. (a) Polarization curves at a scan rate of 5 mV sec^{-1}; (b) Bar chart depicting summary of LSV results; (c) The corresponding Tafel plots; (d) Nyquist electrochemical impedance plots fitted to the RQR equivalent circuit (inset)

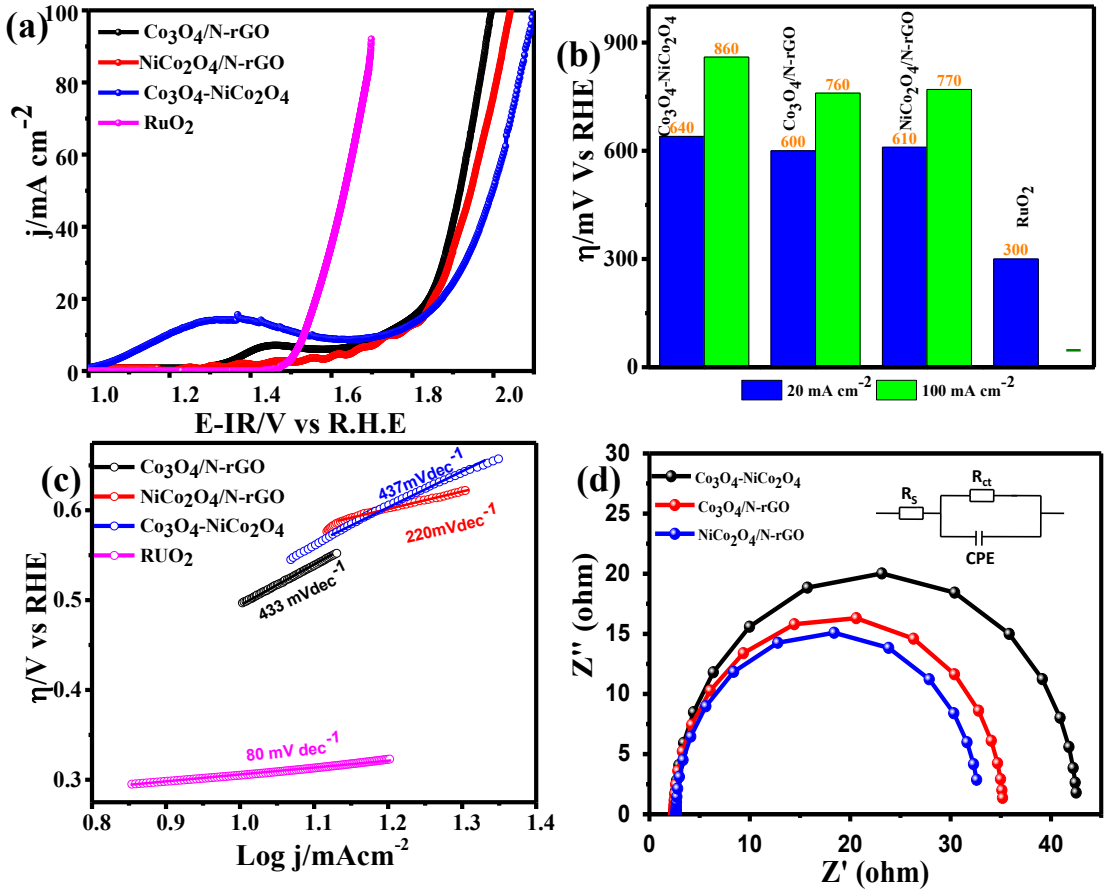

Figure S10. Electrochemical OER characterization of precursor oxide electrocatalysts viz.Co_3O_4-$NiCo_2O_4$, Co_3O_4-rGO, and $NiCo_2O_4$/N-rGO in 1M KOH solution. (a) Polarization curves at a scan rate of 5 mV s^{-1}; (b) Bar chart summarizing the LSV results; (c) The corresponding Tafel plots; (d) EIS Nyquist plots fitted to the RQR equivalent circuit (inset).

General mechanism of hydrogen evolution reaction (HER) over the transition metal sulphides in alkaline medium	General mechanism of Oxygen evolution Reaction (OER) over the transition metal sulphides in alkaline medium
HER on the transition metal sulphide Surface is mainly divided into two steps **In Alkaline medium** Step1: Volmer step $MS + H_2O + e^- \longrightarrow MSH_{ad} + OH^-$ (Metal sulphide) Step 2: Heyrovsky Step $MSH_{ad} + H_2O + e^- \longrightarrow H_2 + OH^- + MS$	**OER On the transition metal sulphide Surface is shown below** **In Alkaline medium** $MS + OH^- \longrightarrow MSOH$ (Metal sulphide) $MSOH + OH^- \longrightarrow MSO + H_2O$ $MSO + MSO \longrightarrow 2MS + O_2$ OR $MSO + OH^- \longrightarrow MSOOH + e^-$ $MSOOH + OH^- \longrightarrow MS + O_2 + H_20$ Overall reaction $4OH^- \longrightarrow 2H_2O + 4e^- + O_2$

Figure S11. General reaction mechanism for water splitting (HER on left and OER on the right)on the surface of transition metal sulphides.

Table S1. Comparison ofHER and OER performance of Co_9S_8-$NiCo_2S_4$/N-rGO and some other noble-metal-free electrocatalysts at 10 mA cm^{-2} in 1.0 M KOH. (j: current density; Ƞ: overpotential)

Catalyst	HER in 1M KOH				OER in 1M KOH				ECSA Analysis	
	Ƞ(J=10 mAcm^{-2}) [mV]	Ƞ (for J=100 mA cm^{-2}) [mV]	Tafel Slope [mV dec^{-1}]	R_{CT} [Ω]	Ƞ (for J=20 mA cm^{-2}) [mV]	Ƞ (for J=100 mA cm^{-2}) [mV]	Tafel Slope [mV dec^{-1}]	R_{CT} [Ω]	Cdl (mF)	ECSA (cm^{-2})
Co_9S_8-$NiCo_2S_4$/N-rGO	149	257	89	9.3	230	362	93	10.5	41.14	1,028.5
Co_9S_8/N-rGO	194	312	91	10.6	282	393	107	16.0	23.33	583.25
$NiCo_2S_4$/N-rGO	257	479	180	13.9	465	690	338	26.3	23.01	575.25
Co_3O_4-$NiCo_2O_4$/N-rGO	312	512	131	10.5	420	650	171	25.3	27.35	683.75
Co_3O_4-$NiCo_2O_4$	537	781	164	35.2	640	880	437	40.1	13.28	332
Co_3O_4/ N-rGO	377	631	125	24	600	760	220	30.0	20.73	518.2
$NiCo_2O_4$/N-rGO	327	556	140	20.9	610	770	433	32.2	22.91	572.75

TableS2. Comparison of full cell water splitting activity of Co_9S_8-$NiCo_2S_4$/N-rGO with other reported bifunctional catalysts in basic medium

Catalysts	Cell Voltage [V] (for J=10 mA cm^{-2})	Electrolyte	Reference
Co_9S_8-$NiCo_2S_4$/N-rGO	1.59	1M KOH	This work
$NiCo_2S_4$ NW/NF	1.63	1M KOH	[9]
CoOSeP@Co	1.74	1M KOH	[10]
Ni5P4/NF	1.69	1M KOH	[11]
CoSe film	1.65	1M KOH	[12]
Co_9S_8-MoS_2	1.67	1M KOH	[13]
CoP@NCHNCs	1.62	1M KOH	[14]
MoS_2-Co_9S_8-NC	1.61	1M KOH	[15]
$NiCo_2S_4$/N-rGO	1.63	1M KOH	[16]
NCT-$NiCo_2S_4$	1.6	1M KOH	[17]
$FeCo_2S_4$-$NiCo_2S_4$	1.51	1M KOH	[18]
P/Pt	>1.8	1M KOH	[11]
RuO_2/ RuO_2	1.45	1M KOH	[19]
Ir-C/Pt-C on EG	1.62	1M KOH	[19]
Pt –C/Pt-C	1.75	1M KOH	[20]

Reference

1 S. Shah, H. Shaikh, S. Farrukh, M. I. Malik, Z. un N. Mughal and S. Bhagat, *RSC Adv.*, 2021, **11**, 19647–19655.

2 A. K. Das, R. K. Layek, N. H. Kim, D. Jung and J. H. Lee, *Nanoscale*, 2014, **6**, 10657–10665.

3 H. Zhang, H. Li, H. Wang, K. He, S. Wang, Y. Tang and J. Chen, *J. Power Sources*, 2015, **280**, 640–648.

4 R. Bhargava, S. Khan, N. Ahmad and M. M. N. Ansari, *AIP Conf. Proc.*, 2018, **1953**, 1–5.

5 Y. Zheng, J. Xu, X. Yang, Y. Zhang, Y. Shang and X. Hu, *Chem. Eng. J.*, 2018, **333**, 111–121.

6 R. Ramachandran, M. Saranya, C. Santhosh, V. Velmurugan, B. P. C. Raghupathy, S. K. Jeong and A. N. Grace, *RSC Adv.*, 2014, **4**, 21151–21162.

7 X. Yang, C. Xiang, Y. Zou, X. Fen, X. Mao, H. Xuebu, J. Zhang and L. Sun, *J. Mater. Res. Technol.*, 2020, **9**, 13718–13728.

8 T. Zhu, G. Zhang, T. Hu, Z. He, Y. Lu, G. Wang, H. Guo, J. Luo, C. Lin and Y. Chen, *J. Mater. Sci.*, 2016, **51**, 1903–1913.

9 A. Sivanantham, P. Ganesan and S. Shanmugam, *Adv. Funct. Mater.*, 2016, **26**, 4661–

4672.

10 Y. F. Jiang, C. Z. Yuan, X. Zhou, Y. N. Liu, Z. W. Zhao, S. J. Zhao and A. W. Xu, *Electrochim. Acta*, 2018, **292**, 247–255.

11 M. Ledendecker, S. Krickcalderõn, C. Papp, H. P. Steinrück, M. Antonietti and M. Shalom, *Angew. Chemie - Int. Ed.*, 2015, **54**, 12361–12365.

12 F. Paquin, J. Rivnay, A. Salleo, N. Stingelin and C. Silva, *J. Mater. Chem. C*, 2015, **3**, 10715–10722.

13 and M. C. Jinman Bai, Tao Meng, Donglei Guo, Shuguang Wang, Baoguang Mao, *ACS Appl. Mater. Interfaces*, 2017, **10**, 1678–1689.

14 Y. Chen, M. Wang, S. Xiang, J. Liu, S. Feng, C. Wang, N. Zhang, T. Feng, M. Yang, K. Zhang and B. Yang, *ACS Sustain. Chem. Eng.*, 2019, **7**, 10912–10919.

15 N. Huang, S. Yan, M. Zhang, Y. Ding, L. Yang, P. Sun and X. Sun, *Electrochim. Acta*, 2019, **327**, 134942.

16 H. S. Lee, J. Pan, G. S. Gund and H. S. Park, *Adv. Mater. interface*, 2020, **7**, 2000138.

17 F. Li, R. Xu, Y. Li, F. Liang, D. Zhang, W. F. Fu and X. J. Lv, *Carbon N. Y.*, 2019, **145**, 521–528.

18 D. Li, Z. Liu, J. Wang, B. Liu, Y. Qin, W. Yang and J. Liu, *Electrochim. Acta*, 2020, **340**, 135957.

19 Y. Dang, T. Wu, H. Tan, J. Wang, C. Cui and P. Kerns, *Energy Environ. Sci.*, 2021, **14**, 5433–5443.

20 N. Jiang, B. You, M. Sheng and Y. Sun, *Angew. Chemie*, 2015, **127**, 6349–6352.